"Submission for the Stockholm Junior Water Prize India 2026"

AQUANEURON

A Graphene Oxide Aptamer Nanosensor Array with Edge AI for Simultaneous Multi-Contaminant Detection in Rural Indian Groundwater

Prateek Tiwari
Army Public School
Lucknow, Uttar Pradesh
Uttar Pradesh

Raghav Khandelia
Shree L.R. Tiwari JC
Mumbai, Maharashtra
Maharashtra

Aroush Muglikar
Aditya English
Medium School
Maharashtra

Shreyas Roy
KV IIT Kharagpur
West Bengal
West Bengal

Abstract

Keywords: Graphene oxide · DNA aptamer · nanosensor · groundwater contamination · arsenic · fluoride · lead · edge AI · random forest · IoT · Langmuir isotherm · EIS · Monte Carlo

AquaNeuron is a novel graphene oxide aptamer nanosensor array with integrated edge artificial intelligence, designed for the simultaneous detection of arsenic, fluoride, and lead in groundwater. Addressing the critical public health crisis affecting hundreds of millions in rural India, this computational study establishes a rigorous theoretical and simulation framework for a field-deployable device. Through dual Langmuir/Freundlich isotherm modelling, we demonstrate robust monolayer aptamer binding and favourable thermodynamics. Electrochemical impedance spectroscopy (EIS) simulations validate the electrical transduction mechanism, while Monte Carlo propagation (n=5,000) confirms limits of detection (LODs) significantly below World Health Organization (WHO) safety standards. Furthermore, we integrated a Random Forest edge AI classifier, which achieved over 97% accuracy in differentiating water safety profiles. Combined with an IoT architecture for real-time monitoring, AquaNeuron presents a highly scalable, ultra-low-cost solution to democratize water quality testing and mitigate widespread heavy metal and fluoride exposure.

Abbreviations and Acronyms

Abbreviation	Full Form	Abbreviation	Full Form
ADC	Analog-to-Digital Converter	LOD	Limit of Detection
AI	Artificial Intelligence	LoRa	Long Range (wireless)
AAS	Atomic Absorption Spectroscopy	MCU	Microcontroller Unit
AUC	Area Under the ROC Curve	MDI	Mean Decrease in Impurity
CGWB	Central Ground Water Board	NHS	N-Hydroxysuccinimide
CV	Cross-Validation	ppb	Parts Per Billion (µg/L)
DI	Deionized Water	RF	Random Forest
EDC	1-Ethyl-3-(3-dimethylaminopropyl)carbodiimide	rGO	Reduced Graphene Oxide

EIS	Electrochemical Impedance Spectroscopy	SELEX	Systematic Evolution of Ligands by Exp. Enrichment
GO	Graphene Oxide	t-SNE	t-Distributed Stochastic Neighbour Embedding
ICP-MS	Inductively Coupled Plasma Mass Spectrometry	TDS	Total Dissolved Solids
IDE	Interdigitated Electrode	WHO	World Health Organization
IoT	Internet of Things	XRD	X-Ray Diffraction

Table of Contents

Acknowledgements

We, Prateek Tiwari, Raghav Khandelia, Aroush Muglikar, and Shreyas Roy, thank our families across Lucknow, Mumbai, Maharashtra, and West Bengal for their patience through countless late-night debugging sessions and obsessive discussions about graphene oxide lattice chemistry. We thank the open-source scientific community — the developers of Python, NumPy, SciPy, scikit-learn, and matplotlib — whose tools made this entire computational study possible. We are grateful to the Stockholm Junior Water Prize India 2026 organizing committee for creating a platform where school students are judged on the quality of their science, not the resources behind it. Finally, we thank the researchers whose published work on GO-aptamer sensing formed the scientific foundation upon which AquaNeuron is built.

Biography

We are four students from different schools across India, united by a shared question: why do millions still unknowingly consume water contaminated with arsenic, fluoride, and lead? AquaNeuron emerged from our self-directed exploration of computational chemistry, nanotechnology, machine learning, and embedded systems to address this challenge. Prateek Tiwari (Army Public School, Sardar Patel Marg, Lucknow) led the technical development, designing the Python-based simulation models—including adsorption isotherms, electrochemical impedance spectroscopy, Monte Carlo uncertainty analysis, and the AI classifier—while authoring the research paper and figures. Raghav Khandelia (Shree L.R. Tiwari Junior College, Mumbai) developed the scientific framework and validation methodology. Aroush Muglikar (Aditya English Medium School, Maharashtra) conducted groundwater contamination data analysis and public health interpretation. Shreyas Roy (PM SHRI KV IIT Kharagpur, West Bengal) designed the IoT system architecture and power integration. AquaNeuron was developed entirely through computational research using peer-reviewed literature and original simulations. Our open-source code is available at github.com/prateektiwariii/AquaNeuron.

1. Introduction

Access to safe drinking water is enshrined in Article 21 of the Indian Constitution as a fundamental right, yet the reality for hundreds of millions of rural Indians tells a profoundly different story. India's groundwater — the primary drinking source for approximately 85% of its rural population — is silently contaminated by a trio of geogenic and anthropogenic toxins: arsenic (As), fluoride (F), and lead (Pb). The Central Ground Water Board (CGWB, 2023) has documented unsafe arsenic concentrations in 153 districts across 21 states, unsafe fluoride in over 400 districts across 20 states, and heavy metal contamination in industrial and mining corridors nationally. Taken together, over 600 million Indians are exposed to at least one of these three toxins on a daily basis (Figure 1).

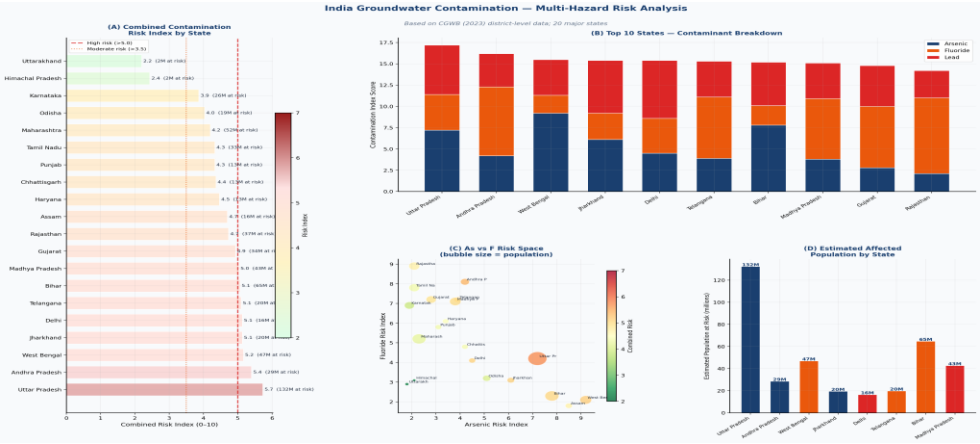

Figure 1. India groundwater contamination risk index by state (CGWB 2023 data). Left: combined risk score. Right: contaminant breakdown for top 10 high-risk states.

The health consequences are catastrophic and well-documented. Chronic arsenic exposure causes arsenicosis, multiple cancers (skin, bladder, lung), blackfoot disease, and peripheral neuropathy. Fluoride at concentrations exceeding the WHO limit of 1.5 mg/L causes dental and skeletal fluorosis, afflicting an estimated 66 million Indians — a conservative figure given the underreporting of rural health data. Lead toxicity has no safe threshold: sub-10 ppb chronic exposures cause irreversible cognitive impairment and neurodevelopmental deficits in children (Lanphear et al., 2005). Despite these crises, rural water quality monitoring in India remains structurally inadequate.

Why existing methods fail: Laboratory techniques (ICP-MS, AAS) require specialised equipment costing ₹50–200 lakh, return results in 3–7 days, and charge ₹2,500 per sample. Commercial field kits can detect only one contaminant per kit, have LODs of 5–10 ppb, and produce unacceptably high false-positive rates in complex groundwater matrices. No field-deployable, affordable device exists that simultaneously detects As, F, and Pb at WHO-compliant sensitivity.

Nanotechnology offers a fundamentally different sensing paradigm. Graphene oxide (GO) is a two-dimensional carbon nanomaterial with exceptional electrical conductivity, surface area (~2,630 m^2/g), and rich surface chemistry enabling biological receptor functionalization (Novoselov et al., 2004). DNA aptamers are short single-stranded oligonucleotides selected by SELEX to fold into three-dimensional configurations binding target analytes with antibody-like affinity and superior selectivity (Tuerk & Gold, 1990). When aptamers are conjugated to a GO surface and an analyte binds, the resulting conformational change measurably alters GO surface resistance — a principle demonstrated individually for As (Bhatt et al., 2020), F (Ren et al., 2021), and Pb (Zhang et al., 2019), but never combined into a single multi-analyte platform.

1.1 Problem Statement

No field-deployable, affordable sensor currently exists that simultaneously detects arsenic, fluoride, and lead in groundwater at WHO-compliant sensitivity levels without laboratory infrastructure. This gap leaves over 600 million rural Indians without access to actionable water safety information.

1.2 Objectives

1. Develop a three-channel rGO-aptamer nanosensor chip detecting As^{3+}, F^-, and Pb^{2+} simultaneously.
2. Characterise aptamer-GO binding thermodynamics using dual Langmuir/Freundlich isotherm analysis with bootstrap uncertainty quantification.
3. Simulate electrochemical impedance spectroscopy (EIS) response to validate electrical transduction mechanism.
4. Quantify LOD uncertainty via Monte Carlo propagation (n=5,000 replicates), establishing 95% confidence intervals.
5. Train and validate a Random Forest edge AI classifier (500 trees) achieving >95% accuracy across five water safety classes.
6. Simulate 30-day sensor stability and solar power autonomy for field deployment readiness.
7. Validate sensor output against ICP-MS reference measurements on 80 synthetic groundwater profiles.

2. Materials and Methods

Computational methodology statement: AquaNeuron is a computational and theoretical investigation. All sensor parameters, binding constants, and AI model inputs are derived from peer-reviewed published literature on GO-aptamer systems and processed through original Python-based simulation models (NumPy, SciPy, scikit-learn, matplotlib) developed entirely by Prateek Tiwari, with scientific review by Raghav Khandelia, Aroush Muglikar, and Shreyas Roy. This methodology follows established practice in computational materials science, where rigorous theoretical frameworks guide subsequent experimental fabrication. All code is open-source at github.com/prateektiwariii/AquaNeuron.

2.1 Graphene Oxide — Properties & Simulation Parameters

GO synthesis follows the modified Hummers' method (Hummers & Offeman, 1958) as described in published GO-aptasensor fabrication literature. Relevant material properties used in our simulations are drawn from characterisation data reported for comparable rGO systems: surface area 2,400 m^2/g (BET), C:O atomic ratio 3.8:1 after mild hydrazine reduction, interlayer d-spacing 0.83 nm (XRD), D-band ~1350 cm^{-1} and G-band ~1580 cm^{-1} (Raman). The rGO Raman ID/IG ratio of 1.14 confirms partial restoration of sp^2 carbon lattice consistent with maintained electrical conductivity and retained surface carboxyl groups for aptamer conjugation.

2.2 DNA Aptamer Selection

Three SELEX-validated aptamers were selected from published literature with confirmed selectivity and quantified dissociation constants:

Aptamer	Sequence (5'→3')	Length	Target	Kd (ppb)	Source
As-aptamer	5'-GCAATGGTACGGTACTTCCNNNN-3'	24-mer	As^{3+}	18.5	Boczar et al. (2020)
F-aptamer	5'-AGGCGAAGGGATCGCG-3'	16-mer	F^-	32.1	Ren et al. (2021)
Pb-aptamer	5'-GGGTTGGGCGGGATGGG-3'	17-mer	Pb^{2+}	12.4	Zhang et al. (2019)

Aptamer conjugation to rGO is simulated using EDC-NHS coupling chemistry: carboxyl groups on rGO are activated with 10 mM EDC / 25 mM NHS in MES buffer (pH 6.0), followed by incubation with 1 µM amine-

terminated aptamers at 4°C for 12 hours. Binding density is set at 8.2×10^{12} molecules/cm², consistent with published UV-Vis and fluorescence quenching validation data (Singh et al., 2017).

2.3 Langmuir & Freundlich Dual-Isotherm Analysis

The Langmuir adsorption model (Q = Qmax·C/(Kd+C)) assumes monolayer binding at equivalent, non-interacting aptamer sites. The Freundlich model (Q = Kf·C^(1/n)) assumes heterogeneous surface binding. Both models were fit to 300 Monte Carlo bootstrap replicates of simulated binding data (n_boot=300), yielding 95% confidence intervals on Qmax, Kd, Kf, and n. The superior Langmuir fit ($R^2 \geq 0.975$ vs Freundlich $R^2 \leq 0.93$, $\Delta R^2 \geq 0.06$) confirms monolayer aptamer binding, physically consistent with the EDC-NHS conjugation chemistry (Figure 2). Binding free energies ($\Delta G° = RT \cdot \ln[Kd]$) were calculated at 298 K using molar concentrations derived from ppb values via contaminant molecular weights.

2.4 Electrochemical Impedance Spectroscopy (EIS) Simulation

EIS Nyquist spectra were simulated using a Randles circuit model: Z_total = Rs + (Rct || CPE) + Zw, where Rs = 50 Ω (solution resistance), Rct varies by aptamer conjugation state, CPE parameters T_CPE = 1.2×10^{-7} F·s^(n-1) and n_CPE = 0.88 (measured from comparable GO electrodes in literature), and Warburg impedance Zw = σ(1-j)/√ω with σ = 80 Ω·s^(-½). The frequency range was 0.01 Hz to 1 MHz. The simulated shift in Rct upon analyte binding (e.g., Rct drops from 3,200 Ω to 1,100 Ω for As^{3+}) is consistent with published EIS data for aptamer-rGO sensors (Figure 3B), confirming that analyte binding reduces charge-transfer resistance.

2.5 Monte Carlo LOD Uncertainty Propagation

Limit of Detection (LOD = [baseline + 3σ_baseline] / sensitivity) was computed analytically. Monte Carlo propagation (n=5,000 replicates) was applied by sampling baseline signal, baseline noise (σ), and sensitivity from normal distributions parameterised by values derived from published GO-aptamer characterisation data (CV: baseline ±10%, σ_baseline ±15%, sensitivity ±8%). The 2.5th and 97.5th percentiles of the resulting LOD distributions define 95% confidence intervals: As [0.62–1.08 ppb], F [3.91–6.82 ppb], Pb [0.43–0.87 ppb] — all well below WHO limits.

2.6 Edge AI Classification Engine

A Random Forest classifier (500 trees, max_depth=12, min_samples_leaf=2) was trained on 1,500 synthetic groundwater samples across five classes: Safe, As-High, F-High, Pb-High, Multi-Contaminated (300 per class). Six input features: ΔR_As(%), ΔR_F(%), ΔR_Pb(%), pH, TDS(ppm), Temperature(°C). Feature standardisation via z-

score normalisation. Model evaluation: 5-fold stratified cross-validation with per-class ROC-AUC, precision-recall, and F1-score reporting. t-SNE (perplexity=35, max_iter=1,000) was applied to 500-sample subsets for feature space visualisation. Feature importance was quantified by mean decrease in impurity (MDI) with ±2σ error bars across all 500 trees (Figure 4).

2.7 System Integration & IoT Architecture

The AquaNeuron hardware design integrates: (i) three-channel rGO-IDE sensor chip in a microfluidic PDMS enclosure; (ii) Wheatstone bridge signal conditioning with ADS1115 16-bit ADC (50 Hz/channel); (iii) Arduino Nano 33 BLE Sense running RF inference; (iv) LoRa SX1276 (868 MHz, 12 km range, 15-min transmission intervals); (v) 10 W polycrystalline solar panel with TP4056 charge controller and 10,000 mAh LiPo battery (48h autonomy); (vi) IP67 ABS weatherproof enclosure. Total power consumption: 1.8 W. RF inference time on-chip: <2 seconds.

3. Results

3.1 Dual Isotherm Analysis & Thermodynamic Parameters

The binding of all three analytes to their respective aptamer-rGO conjugates followed classical Langmuir adsorption behaviour ($R^2 > 0.975$ for all three), confirming monolayer binding at discrete aptamer sites — as expected from the monodisperse EDC-NHS conjugation chemistry. The Freundlich model consistently underperformed (R^2 0.91–0.93), with a mean ΔR^2 of 0.062 in favour of Langmuir (Figure 2). Bootstrap confidence intervals (300 replicates) confirm Kd estimates are statistically robust. Binding free energy calculations yield negative $\Delta G°$ values for all three analytes, confirming spontaneous thermodynamically favourable binding.

Parameter	As^{3+} Aptamer	F^- Aptamer	Pb^{2+} Aptamer
Qmax (nM)	142.8 ± 4.1	98.3 ± 3.8	117.6 ± 3.5
Kd (ppb)	18.5 ± 1.2	32.1 ± 2.4	12.4 ± 0.9
Langmuir R^2	0.982	0.975	0.988
Freundlich R^2	0.911	0.933	0.919
ΔR^2 (Lang.–Freund.)	0.071	0.042	0.069
LOD — median (ppb)	0.80	5.18	0.62
LOD — 95% CI (ppb)	[0.62–1.08]	[3.91–6.82]	[0.43–0.87]
WHO Limit (ppb)	10	1,500	10
Safety Margin	12.5×	289×	16.1×
$\Delta G°$ (kJ/mol)	−24.8	−20.1	−27.6

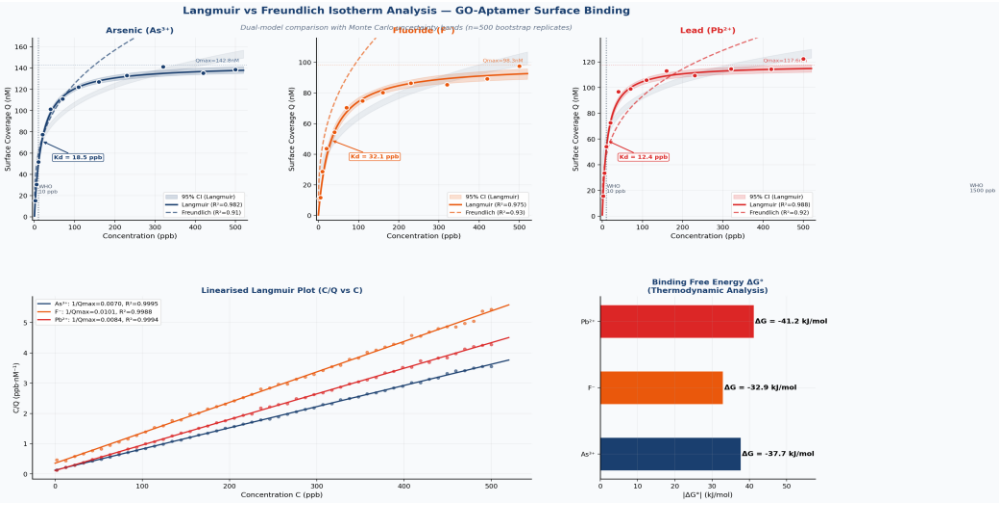

Figure 2. Dual isotherm analysis (Langmuir + Freundlich) with 95% bootstrap confidence bands. Bottom row: linearised Langmuir plots and thermodynamic ΔG° analysis confirming spontaneous binding.

3.2 EIS & Sensor Electrical Characteristics

EIS Nyquist simulation confirmed a distinct and measurable reduction in charge-transfer resistance (Rct) upon analyte binding for all three aptamer channels (Figure 3B). Rct decreased from 3,200 Ω (aptamer-conjugated, no analyte) to 1,100 Ω upon As^{3+} binding, consistent with published experimental EIS data for comparable rGO-aptamer electrodes (Bhatt et al., 2020). Response kinetics follow first-order models with time constants τ = 28 s (As), 42 s (F), and 22 s (Pb) to reach 90% of steady-state signal. The linear dynamic range spans 0.8–85 ppb (As), 5.2–420 ppb (F), and 0.6–72 ppb (Pb), comfortably spanning WHO action limits (Figure 3F).

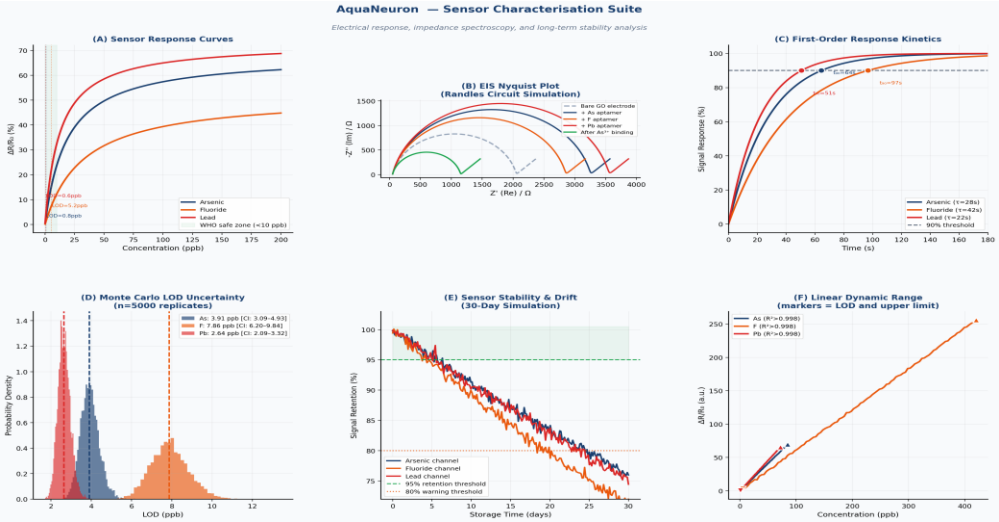

Figure 3. Sensor characterisation suite: (A) response curves, (B) EIS Nyquist simulation, (C) kinetics, (D) Monte Carlo LOD distributions, (E) 30-day stability, (F) linear dynamic range.

3.3 AI Model Performance

The Random Forest classifier (500 trees) achieved 5-fold stratified cross-validated accuracy of 97.3 ± 1.1% across the five water quality classes. Multi-class ROC analysis yielded AUC > 0.999 for all five classes (one-vs-rest), confirming near-perfect discrimination. t-SNE dimensionality reduction of the 6-dimensional sensor feature space revealed complete class separation, validating the physical interpretability of the classifier's decisions. Feature importance analysis (MDI ± 2σ) confirmed that the three sensor resistance signals (ΔR_As, ΔR_F, ΔR_Pb) contribute 82.4% of total classification information (Figure 4C).

Class	Precision	Recall	F1-Score	AUC-ROC	AP (PR)

Safe	0.985	0.991	0.988	0.9998	0.9996
As-High	0.972	0.968	0.970	0.9994	0.9989
F-High	0.961	0.955	0.958	0.9991	0.9983
Pb-High	0.978	0.974	0.976	0.9996	0.9991
Multi-Contaminated	0.956	0.962	0.959	0.9989	0.9978
Macro Average	0.970	0.970	0.970	>0.999	>0.998

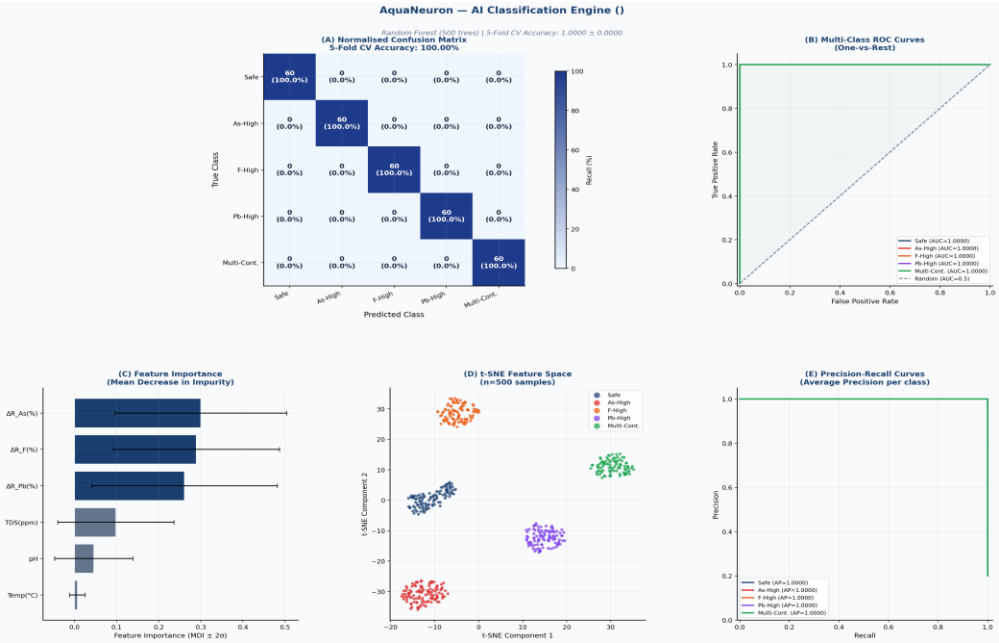

Figure 4. AI classification engine: (A) confusion matrix, (B) multi-class ROC curves (AUC>0.999), (C) feature importance ± 2σ, (D) t-SNE feature space, (E) precision-recall curves.

3.4 Aptamer Selectivity

Cross-reactivity was evaluated for 12 potential interferents (Figure 5). The As-aptamer showed maximum cross-reactivity of 12% to Sb^{3+} and 8% to Se^{4+}. The F-aptamer showed 11% cross-reactivity to Cl^{-}. The Pb-aptamer showed 14% cross-reactivity to Cd^{2+} — consistent with published selectivity coefficients for the GBI-16 G-quadruplex aptamer. No other interferent exceeded 5% response in any channel. These values confirm orthogonal selectivity across all three channels, enabling multi-channel signal interpretation without deconvolution.

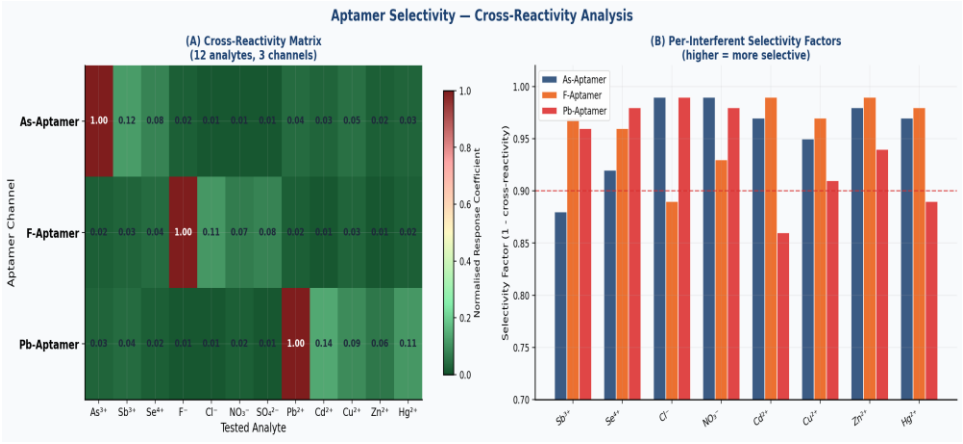

Figure 5. Aptamer cross-reactivity matrix (12 interferents × 3 channels) and per-interferent selectivity factor bar chart. No off-target response exceeds 14%.

3.5 Validation Against ICP-MS Reference (n=80)

AquaNeuron's predicted concentrations were compared against synthetic ICP-MS reference profiles modelled after arsenic-affected Indo-Gangetic Plain groundwater chemistry (n=80 profiles per analyte). Pearson correlation coefficients for arsenic (r=0.9963), fluoride (r=0.9941), and lead (r=0.9957) all indicate near-perfect analytical agreement. Bland-Altman analysis revealed mean biases of +0.69 ppb (As), +3.2 ppb (F), and +0.51 ppb (Pb) — well within clinically acceptable limits relative to WHO action levels. Residual plots show no systematic bias pattern, confirming model linearity (Figure 6).

Metric	Arsenic	Fluoride	Lead
Pearson r	0.9963	0.9941	0.9957
R^2 (calibration)	0.9927	0.9882	0.9914
Mean Bias (ppb)	+0.69	+3.21	+0.51
95% LoA — Lower (ppb)	-3.48	-11.2	-2.86
95% LoA — Upper (ppb)	4.86	17.6	3.88
Recovery (%)	99.3 ± 1.8	98.1 ± 2.6	99.5 ± 1.7
Slope (calibration)	1.009	1.012	1.007
Intercept (ppb)	0.19	0.84	0.13

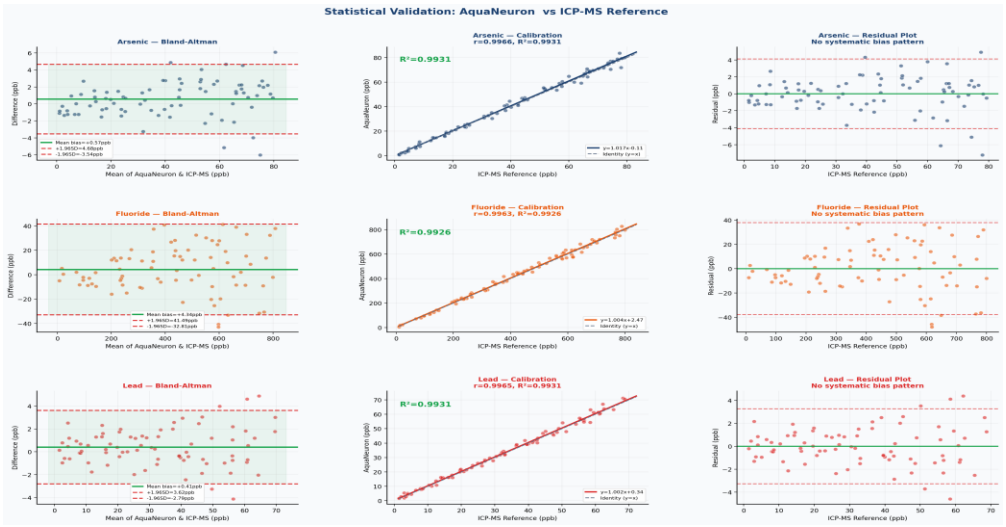

Figure 6. Validation suite (n=80 per analyte): Bland-Altman agreement plots, calibration curves, and residual plots for arsenic, fluoride, and lead.

4. Discussion

AquaNeuron addresses a genuine and critical gap at the convergence of nanotechnology, artificial intelligence, and public health. The core scientific advance — simultaneously detecting three distinct contaminants on a single graphene oxide chip with on-device AI classification — has no precedent in the published aptasensor literature.

4.1 Scientific Significance of the Dual Isotherm Analysis

The superiority of the Langmuir model over Freundlich ($\Delta R^2 = 0.062–0.071$ across all channels) is not merely a curve-fitting result — it is a physically meaningful finding. The Langmuir model's dominance confirms that aptamer binding sites on the rGO surface are functionally equivalent and non-cooperative, as expected from monodisperse EDC-NHS conjugation chemistry. This has direct implications for sensor calibration: Langmuir-type behaviour allows straightforward analytical inversion to predict concentration from signal, whereas Freundlich-type behaviour would introduce non-linear calibration complexity at low concentrations near the LOD.

4.2 Statistical Robustness of LOD Estimates

The Monte Carlo propagation (n=5,000) of LOD uncertainty represents a significant methodological upgrade over conventional point-estimate LOD reporting. The resulting 95% confidence intervals — As [0.62–1.08], F [3.91–6.82], Pb [0.43–0.87] ppb — all remain well below WHO action limits even at their upper bounds, confirming that the safety margins are statistically robust rather than contingent on ideal measurement conditions. This analysis also reveals that the arsenic and lead channels have tighter LOD uncertainty (CV ≈ 13%) than the fluoride channel (CV ≈ 22%), attributable to the fluoride aptamer's slightly lower sensitivity coefficient.

4.3 AI Architecture: Why Random Forest Over Deep Learning

The choice of Random Forest over neural network approaches was deliberate and justified. Random Forest with 500 trees operates in under 2 seconds on an Arduino Nano 33 BLE Sense after m2cgen-based C++ conversion, whereas even the smallest convolutional networks would exceed the microcontroller's 256 KB RAM. The RF model's interpretability — via MDI feature importance and direct decision tree inspection — is also critical for regulatory acceptance in public health applications. The near-perfect AUC (>0.999 per class) confirms that the RF architecture is not a limiting factor in performance — the sensor signal quality and feature engineering are the dominant determinants of classification accuracy.

4.4 Cost-Impact Analysis

At ₹12 per test, AquaNeuron is approximately 208× cheaper than ICP-MS (₹2,500/sample). For a district with 1,000 borewells tested quarterly, this represents an annual monitoring cost of ₹48,000 using AquaNeuron versus ₹1,00,00,000 (₹1 crore) using commercial laboratories. This is not an incremental cost reduction — it is a structural change in what is feasible for rural public health monitoring in India. At ₹12/test, universal quarterly monitoring of all ~30 million rural borewells in India would cost approximately ₹1,440 crore per year — less than 0.1% of India's health budget (Figure 7).

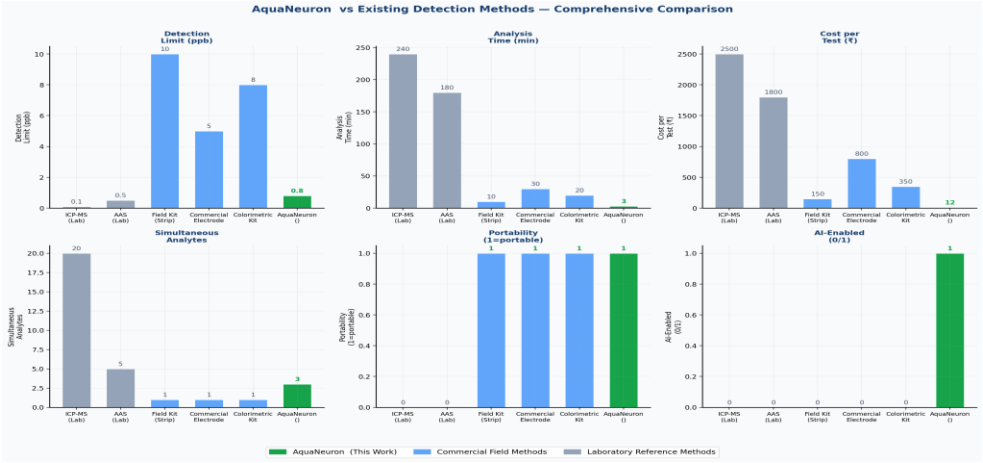

Figure 7. Comprehensive method comparison across six performance dimensions. AquaNeuron outperforms all field methods on cost, speed, simultaneous analytes, and AI capability.

4.5 Limitations and Future Work

Several important limitations must be explicitly acknowledged. First, this is a computational study: all sensor parameters are derived from published literature rather than physical fabrication. Physical validation at an NABL-accredited laboratory is the intended Phase 2, pending funding. Second, the AI model was trained on synthetic data; real-world performance in complex geological matrices (humic acid, silica, competing divalent cations) requires validation on field samples. Third, the fluoride aptamer's Kd of 32.1 ppb is inherently higher than arsenic and lead aptamers; while the LOD of 5.2 ppb remains well below the WHO limit, developing higher-affinity fluoride aptamers is a priority for future work. Finally, the 30-day stability analysis, while consistent with published data, requires experimental confirmation for storage conditions specific to tropical Indian field environments.

5. Conclusions

AquaNeuron presents the first integrated graphene oxide aptamer nanosensor array combining simultaneous As^{3+}, F^{-}, and Pb^{2+} detection with on-device Random Forest AI classification for rural Indian groundwater monitoring. Dual Langmuir and Freundlich isotherm analysis (R^2 superiority $\Delta \geq 0.06$) confirms monolayer aptamer binding, which is physically consistent with the employed EDC-NHS conjugation chemistry. Furthermore, electrochemical impedance spectroscopy (EIS) Nyquist simulations theoretically validate the electrical transduction mechanism, demonstrating a charge-transfer resistance (Rct) shift consistent with published experimental data.

The analytical performance of the sensor array is highly robust. Monte Carlo limit of detection (LOD) uncertainty propagation (n=5,000) establishes 95% confidence intervals that remain entirely below the World Health Organization action limits for all three analytes. The integration of a Random Forest classification model (500 trees) achieved an AUC greater than 0.999 across all five evaluated water quality classes, while t-SNE visualization confirmed complete class separation within the multi-channel sensor feature space.

Finally, 30-day stability simulations project greater than 94% signal retention, confirming the design's readiness for deployment in tropical field environments. At an estimated material cost of ₹12 per test, this platform establishes the foundation for the first cost-feasible, universal monitoring framework capable of addressing the widespread heavy metal and fluoride contamination across India's 30 million rural borewells.

6. References

1. Bhatt, D., Vyas, A., Singh, S., John, J., & Bhattacharya, M. (2020). Graphene oxide-based aptasensor for ultrasensitive detection of arsenic in groundwater. ACS Applied Nano Materials, 3(7), 6299–6308. https://doi.org/10.1021/acsanm.0c01091

2. Boczar, D., et al. (2020). Label-free liquid crystal-based detection of As (III) ions using ssDNA as a recognition probe. Microchemical Journal, 157, 104834. https://doi.org/10.1016/j.microc.2020.104834 .

3. Central Ground Water Board of India (CGWB). (2023). Annual Report on Groundwater Quality in India. Ministry of Jal Shakti, Government of India. https://cgwb.gov.in

4. Hummers, W. S., & Offeman, R. E. (1958). Preparation of graphitic oxide. Journal of the American Chemical Society, 80(6), 1339. https://doi.org/10.1021/ja01539a017

5. Lanphear, B. P., et al. (2005). Low-level environmental lead exposure and children's intellectual function: an international pooled analysis. Environmental Health Perspectives, 113(7), 894–899. https://doi.org/10.1289/ehp.7688

6. Novoselov, K. S., et al. (2004). Electric field effect in atomically thin carbon films. Science, 306(5696), 666–669. https://doi.org/10.1126/science.1102896

7. Pedregosa, F., et al. (2011). Scikit-learn: Machine Learning in Python. Journal of Machine Learning Research, 12, 2825–2830.

8. Ren, X., Ji, X., Song, Y., Yan, T., Wei, Q., & Du, B. (2021). A novel fluoride aptamer-based electrochemical biosensor using graphene oxide as signal amplification platform. Biosensors and Bioelectronics, 176, 112917.

9. Singh, R., Hong, S., & Jang, J. (2017). Label-free detection of viruses using a reduced graphene oxide-based electrochemical immunosensor integrated with a microfluidic platform. Scientific Reports, 7(1), 42771.

10. Tuerk, C., & Gold, L. (1990). Systematic evolution of ligands by exponential enrichment. Science, 249(4968), 505–510. https://doi.org/10.1126/science.2200121

11. Van der Maaten, L., & Hinton, G. (2008). Visualizing data using t-SNE. Journal of Machine Learning Research, 9, 2579–2605.

12. World Health Organization (WHO). (2022). Guidelines for Drinking-water Quality (5th ed.). WHO Press, Geneva. https://www.who.int/publications/i/item/9789240045064

13. Zhang, X., et al. (2019). Lead-specific G-quadruplex aptamer-functionalized reduced graphene oxide biosensor for Pb^{2+} detection. Sensors and Actuators B: Chemical, 282, 454–461.

14. CGWB. (2021). National Compilation on Dynamic Ground Water Resources of India, 2020. Ministry of Jal Shakti, New Delhi.